

Entanglement Spectrum Dynamics as a Probe for Non-Hermitian Bulk-Boundary Correspondence in Systems with Periodic Boundaries

Pablo Bayona-Pena,¹ Ryo Hanai,¹ Takashi Mori,² and Hisao Hayakawa¹

¹*Center for Gravitational Physics and Quantum Information,*

Yukawa Institute for Theoretical Physics, Kyoto University, Kyoto 606-8502, Japan

²*Department of Physics, Keio University, 3-14-1 Hiyoshi, Yokohama, 223-8522, Japan*

(Dated: September 12, 2024)

It has recently been established that open quantum systems may exhibit a strong spectral sensitivity to boundary conditions, known as the non-Hermitian/Liouvillian skin effect (NHSE/LSE), making the topological properties of the system boundary-condition sensitive. In this Letter, we ask the query: Can topological phase transitions of open quantum systems, captured by *open* boundary conditioned invariants, be observed in the dynamics of a system in a *periodic* boundary condition, even in the presence of NHSE/LSE? We affirmatively respond to this question, by considering the quench dynamics of entanglement spectrum in a periodic open quantum fermionic system. We demonstrate that the entanglement spectrum exhibits zero-crossings only when this *periodic* system is quenched from a topologically trivial to non-trivial phase, defined from the spectrum in *open* boundary conditions, even in systems featuring LSE. Our results reveal that non-Hermitian topological phases leave a distinctive imprint on the unconditional dynamics within a subsystem of fermionic systems.

Introduction.- The recent expansion of phases of matter into the non-Hermitian realm has significantly broadened our understanding of free fermionic systems [1–3]. The presence of non-Hermiticity, which generally arises from the exchange of energy and/or particles of a system with the environment, leads to various exotic phenomena. A paradigmatic example is the emergence of extreme spectral sensitivity to boundary conditions, often referred to as the *non-Hermitian skin effect* (NHSE) [4–6, 10–14], or *Liouvillian skin effect* (LSE) in the context of open quantum systems [6, 7, 18–21], see also [8, 9] for related results in interacting many-body systems. In the presence of NHSE/LSE, the system exhibits exponential localization of eigenstates near its boundaries. This poses a challenge to the conventional understanding of bulk-boundary correspondence: the presence of topological edge states in open boundary conditions (OBC) cannot be inferred from the topological invariant of the Bloch Hamiltonian [4, 5]. In this situation, one must extend the conventional Bloch band theory to incorporate complex-valued wave vectors in order to identify topological invariants in OBC [4, 5]. This is known as the non-Hermitian bulk-boundary correspondence.

Let us remark, however, a somewhat obvious point that for systems subject to periodic boundary conditions (PBC), the topological transition point is determined by the Bloch Hamiltonian even in the presence of NHSE/LSE. It is tempting to expect that no sign of topological invariants defined from the OBC spectrum can be extracted from the PBC system.

In this Letter, in sharp contrast to this naïve expectation, we show that there are cases where OBC topological invariants can be extracted from the dynamics of the PBC system. This is achieved by examining the quench dynamics of the entanglement spectrum (ES).

Initially recognized in the context of a fractional quantum Hall insulator [24] and later formalized for free fermionic [25] and one-dimensional systems [26], the ES has since played a pivotal role in understanding topological phases of both non-interacting and interacting systems. In highly non-equilibrium states, the ES serves as a dynamical probe for wavefunction topology [27–29]. Recent investigations have even extended its applicability to open quantum systems, where the real line-gap topology was shown to be detectable through the quench dynamics of ES [30–32]. However, these works considered systems that do not exhibit LSE [30–32], leaving the effect of boundary conditions sensitivity on the dynamics of ES unclear.

We examine in this Letter an open quantum fermionic lattice exhibiting LSE and show that the dynamics of the ES can serve as a probe for topological phases defined from the OBC spectrum, even when the physical system is in PBC. In particular, we numerically analyze an open quantum model whose dynamics is governed by a dynamical matrix identical to the non-Hermitian Su-Schrieffer-Heeger (SSH) model, a paradigmatic model exhibiting NHSE/LSE [4–6, 19, 21] and demonstrate that in PBC systems, topological phases defined from the OBC spectrum of Lindbladians are discernible through mode crossings of the ES during quench dynamics. As the ES in open free fermion systems can be computed from a two-point correlation function of a subsystem [36], our proposal to detect the non-Hermitian bulk-boundary correspondence does not require post-selection.

We remark that conventional observables such as the correlation functions and steady-state density profile are *not* generically affected by NHSE/LSE, [15–21]. Intuitively, this is due to the locality of the system: the system’s response to an external perturbation applied in the

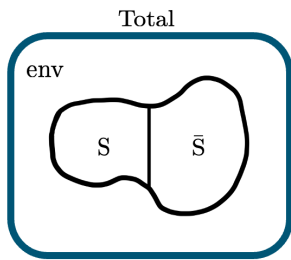


Figure 1. Illustration of tri-partition of an open quantum system. The bipartite relevant system ($S + \bar{S}$) is allowed to interact with the environment (env). We focus on the coarse-grained dynamics of the relevant system after tracing out the environmental degrees of freedom $\hat{\rho} = \text{Tr}_{\text{env}}[\hat{\rho}_{\text{tot}}]$.

bulk is unaffected by the boundary condition unless the effect reaches the boundary before it dissipates. Our finding here seems to contradict these previous results, but it does not: the ES is a highly non-local quantity (for macroscopically large subsystem sizes that we consider in this Letter), making it possible to catch the (non-local) spectral sensitivity to boundary conditions stemming from LSE.

The model.— We investigate the dynamics of an open quantum system, illustrated in Fig. 1, where a free fermionic system ($S + \bar{S}$) is linearly coupled to a Markovian environment (env). After integrating out the environmental degrees of freedom, the reduced density matrix $\hat{\rho} = \text{Tr}_{\text{env}}\hat{\rho}_{\text{tot}}$ is governed by a quadratic Gorini–Kossakowski–Sudarshan–Lindblad (GKSL) equation [22, 23], given by,

$$\partial_t \hat{\rho}(t) = -i[\hat{H}, \hat{\rho}(t)] + \sum_{\alpha} \mathcal{D}[\hat{L}_{\alpha}] \hat{\rho}(t) + \sum_{\alpha} \mathcal{D}[\hat{G}_{\alpha}] \hat{\rho}(t), \quad (1)$$

where $\hat{H} = \sum_{i,j=1}^L H_{i,j} \hat{c}_i^{\dagger} \hat{c}_j$ is the Hamiltonian of the relevant system ($S + \bar{S}$). Here, \hat{c}_i^{\dagger} and \hat{c}_i are creation and annihilation operators of fermions at site i , respectively. The dissipation arising from the coupling of the system to the Markovian reservoir is described by $\mathcal{D}[\hat{M}] \hat{\rho} := \hat{M} \hat{\rho} \hat{M}^{\dagger} - \frac{1}{2} \{ \hat{M}^{\dagger} \hat{M}, \hat{\rho}(t) \}$. Each coupling to the Markovian reservoir, labeled by α (see Fig. 2(a)), induces incoherent addition or removal of particles and is described by linear jump operators, $\hat{L}_{\alpha} = \sum_i \ell_i^{\alpha} \hat{c}_i$ and $\hat{G}_{\alpha} = \sum_i g_i^{*\alpha} \hat{c}_i^{\dagger}$, respectively, where ℓ_n^{α} and g_n^{α} are complex numbers.

According to the tenfold way classification of quadratic fermionic Lindbladians [34], the entire topology of a quadratic Lindbladian can be characterized by the topological invariants of a non-Hermitian operator \hat{H}_{eff} [19]:

$$\hat{H}_{\text{eff}} := \hat{H} - \frac{i}{2}(\hat{L} + \hat{G}), \quad (2)$$

where $\hat{L} = \sum_{\alpha} \hat{L}_{\alpha}^{\dagger} \hat{L}_{\alpha}$, and $\hat{G} = \sum_{\alpha} \hat{G}_{\alpha} \hat{G}_{\alpha}^{\dagger}$. We note that \hat{H}_{eff} is different from the conditional Hamiltonian

$\hat{H}_{\text{cond}} = \hat{H} - (i/2)(\hat{L} - \hat{G})$ that governs the dynamics of null-jump processes [6, 18–20, 35].

ES crossings as a non-Hermitian bulk-boundary correspondence indicator.— To dynamically detect the non-Hermitian bulk-boundary correspondence, we propose examining the ES dynamics after a dissipative quench. As depicted in Fig. 1, we partition the relevant system ($S + \bar{S}$) further into the subsystem $S = \{1, 2, \dots, M\}$ and its complement $\bar{S} = \{M + 1, M + 2, \dots, L\}$. The reduced density matrix of the subsystem can be written as $\hat{\rho}_S = \text{Tr}_{\bar{S}} \hat{\rho} = (1/Z_S) e^{-\hat{H}_S}$ with $Z_S = \text{Tr}_S[e^{-\hat{H}_S}]$, where $\text{Tr}_{S(\bar{S})}$ denotes the trace over the subregion $S(\bar{S})$. We refer to the spectrum of \hat{H}_S as the ES ϵ_l , the central quantity of interest. Using the property that $\hat{\rho}_S$ is Gaussian, the entanglement Hamiltonian can be decomposed as $\hat{H}_S = \sum_l \epsilon_l \hat{f}_l^{\dagger} \hat{f}_l$, where \hat{f}_l is a fermionic annihilation operator of the l -th eigenmode. In the absence of the system-environment coupling, this recovers the conventional definition of the ES for closed fermionic systems, which is known to successfully detect bulk-boundary correspondence [24–26].

References [27–32] considered the situation where they first prepared a state corresponding to the ground state of a Hamiltonian in the trivial phase followed by a sudden change in the parameters. They showed that when the post-quench Hamiltonian has a topologically non-trivial (trivial) ground state, (no) zero-crossings of the ES occur.

We investigate below a similar setup where we also quench the system from a topologically trivial to a non-trivial or trivial state in an open quantum system governed by Eq. (1). Importantly, the topology of our system is characterized by the non-Hermitian effective Hamiltonian \hat{H}_{eff} , given by Eq. (2), that exhibits NHSE. We find that an analogous phenomenon to the closed-system counterpart occurs, which surprisingly reflects the topology of an *OBC* system even when the system itself is in *PBC*: physically traversing the system is unnecessary to detect topological phases of \hat{H}_{eff} defined under open boundary conditions.

Practically, in our quadratic system, the ES can be computed from the covariance matrix $\mathbf{C}(t)$, whose (j, i) component is given by the spatial correlation function $[\mathbf{C}]_{j,i}(t) := \text{Tr}_{S+\bar{S}}[\hat{\rho}(t) \hat{c}_i^{\dagger} \hat{c}_j]$ [36]. By taking advantage of the property that the density matrix is always Gaussian (as long as we take the initial state to be Gaussian) and Wick’s theorem applies as a result, the ES can be derived from the spectrum of the covariance matrix \mathbf{C}_{SS} in the subsystem S defined as the correlation matrix \mathbf{C} whose indices are restricted to the region S ,

$$[\mathbf{C}_{SS}]_{j,i}(t) := \text{Tr}_{S+\bar{S}}[\hat{\rho}(t) \hat{c}_i^{\dagger} \hat{c}_j]; \quad (i, j) \in S, \quad (3)$$

which can be expressed using the reduced density matrix of the subsystem S as $[\mathbf{C}_{SS}]_{j,i}(t) = \text{Tr}_S[\hat{\rho}_S(t) \hat{c}_i^{\dagger} \hat{c}_j]$. Letting $\xi_l(t)$ be the eigenspectrum of $\mathbf{C}_{SS}(t)$, one finds the relation between $\xi_l(t)$ and the ES $\epsilon_l(t)$ [36] (See Supple-

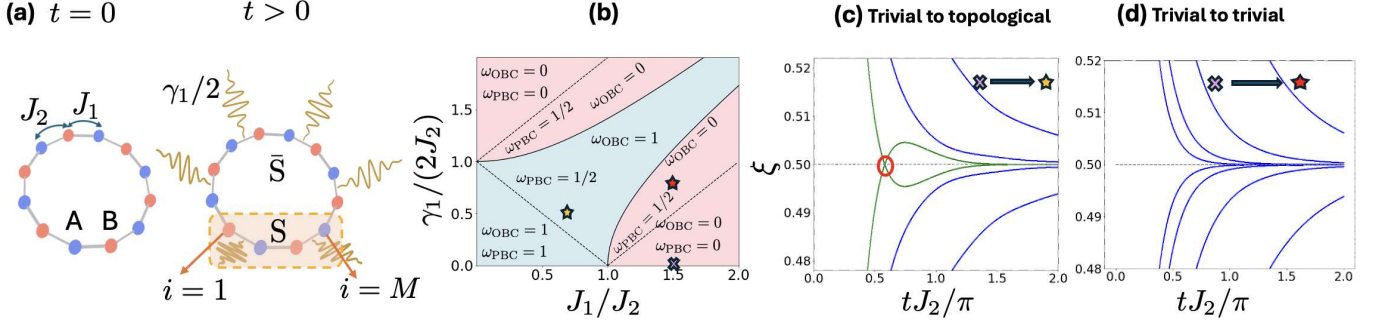


Figure 2. (a) The system is initially prepared in the trivial ground state of the SSH model [33] in PBC with no dissipation. Then, at $t > 0$, the relevant system (S+S) is driven out of its initial state by an abrupt change of the hopping parameters J_1, J_2 and a correlated dissipation with rate γ_1 given by Eq. (8) is simultaneously turned on. The relevant system evolves according to the GKLS equation Eq. (1) in PBC. (b) Phase diagram of the Lindbladian SSH model Eq. (11). Topological phase transitions are separated by the solid and dotted lines for OBC and PBC, respectively. (c) Trivial to topological quenches for both OBC and PBC spectrum ($\omega_{\text{OBC}} = 1, \omega_{\text{PBC}} = 1/2$) ($J_1/J_2, \gamma_1/(2J_2)$) = (0.7, 0.5). The green lines represent the four eigenvalues, $\xi_i(t)$, of the covariance matrix $\mathbf{C}_{\text{SS}}(t)$ that are closest to the zero energy entanglement value $\xi = 0.5$ during the time evolution. The other eigenvalues are shown in blue. Four ES eigenvalues cross $\xi = 0.5$ as they decay. (d) Trivial to trivial quenches for OBC spectrum ($\omega_{\text{OBC}} = 0$) ($J_1/J_2, \gamma_1/(2J_2)$) = (1.5, 0.8) but topological for PBC spectrum ($\omega_{\text{PBC}} = 1/2$). All the eigenvalues, $\xi_i(t)$, of $\mathbf{C}_{\text{SS}}(t)$ are shown in blue. All eigenvalues decay to $\xi = 0.5$ without crossing it. For both cases, we set the initial state to be the (trivial) ground state at $(J_1/J_2, \gamma_1/(2J_2)) = (1.5, 0)$, the system size $L = 20$, and the size of subsystem S is $M = 10$ sites. Note crucially that, while the ES dynamics reflect the OBC spectrum, our physical system is in PBC.

mental Materials (SM) [35]):

$$\xi_i(t) = \frac{1}{e^{\epsilon_i(t)} + 1}. \quad (4)$$

An entanglement zero mode with $\epsilon_i = 0$ corresponds to $\xi_i = 0.5$. To investigate the dynamics of ξ_i , we derive from Eq. (1) the following equation for the covariance matrix dynamics [19, 20]:

$$i\partial_t \mathbf{C}(t) = \mathbf{H}_{\text{eff}} \mathbf{C}(t) - \mathbf{C}(t) \mathbf{H}_{\text{eff}}^\dagger + i\mathbf{G}, \quad (5)$$

where $[\mathbf{G}]_{i,j} = \sum_\alpha g_i^{*\alpha} g_j^\alpha$ and $[\mathbf{H}_{\text{eff}}]_{i,j} = H_{i,j} - i/2 \sum_\alpha (\ell_i^{*\alpha} \ell_j^\alpha + g_i^{*\alpha} g_j^\alpha)$. g_i^α and ℓ_i^α are complex numbers.

Lindbladian SSH model. To be specific, we consider the following system exhibiting LSE [4, 21] (Fig. 2(a)). For the system Hamiltonian, we consider the tight-binding Hamiltonian

$$\hat{H} = \sum_j \left(J_1 \hat{c}_{A,j}^\dagger \hat{c}_{B,j} + J_2 \hat{c}_{B,j}^\dagger \hat{c}_{A,j+1} + J_3 \hat{c}_{A,j+1}^\dagger \hat{c}_{B,j} \right) + h.c. \quad (6)$$

For $J_3 = 0$, the Hamiltonian reduces to the SSH model [33]. The dissipation of our model is given by the following jump operators for $j = 1, 2, \dots, N$ (see Fig. 2 (a)):

$$\hat{L}_{j,1} = \sqrt{\frac{\gamma_1}{2}} (\hat{c}_{A,j} + i\hat{c}_{B,j}), \quad (7)$$

$$\hat{G}_{j,1} = \sqrt{\frac{\gamma_1}{2}} (\hat{c}_{A,j}^\dagger - i\hat{c}_{B,j}^\dagger), \quad (8)$$

$$\hat{L}_{j,2} = \sqrt{\frac{\gamma_2}{2}} (\hat{c}_{A,j+1} + i\hat{c}_{B,j}), \quad (9)$$

$$\hat{G}_{j,2} = \sqrt{\frac{\gamma_2}{2}} (\hat{c}_{A,j+1}^\dagger - i\hat{c}_{B,j}^\dagger). \quad (10)$$

Here, we have chosen the dissipators such that $\hat{L}_{j,s=1,2}^\dagger = \hat{G}_{j,s=1,2}$, ensuring the system reaches an infinite-temperature state at the long-time limit. The ES asymptotically converges to zero $\epsilon_n = 0$ ($\xi_n = 0.5$), avoiding the ES from crossing zero for trivial reasons with no topological origin [30, 37].

Equations (6)-(10) yield the effective Hamiltonian

$$\begin{aligned} \hat{H}_{\text{eff}} = \sum_j & \left[\left(J_1 \hat{c}_{A,j}^\dagger \hat{c}_{B,j} + J_2 \hat{c}_{B,j}^\dagger \hat{c}_{A,j+1} \right. \right. \\ & \left. \left. + J_3 \hat{c}_{A,j+1}^\dagger \hat{c}_{B,j} \right) + h.c. \right] + \sum_j \left(\frac{\gamma_1}{2} (\hat{c}_{A,j}^\dagger \hat{c}_{B,j} - \hat{c}_{B,j}^\dagger \hat{c}_{A,j}) \right. \\ & \left. + \frac{\gamma_2}{2} (\hat{c}_{B,j}^\dagger \hat{c}_{A,j+1} - \hat{c}_{A,j+1}^\dagger \hat{c}_{B,j}) \right) - i \sum_i \gamma_i \hat{n}_i, \end{aligned} \quad (11)$$

with $\hat{n}_i := \sum_j [\hat{c}_{A,j}^\dagger \hat{c}_{A,j} + \hat{c}_{B,j}^\dagger \hat{c}_{B,j}]$, which is the non-Hermitian SSH model well studied in the literature (except for the constant shift in the imaginary axis that does not affect its topological features) that is known to exhibit NHSE [33]. For PBC, the Hamiltonian \hat{H}_{eff} can be expressed as $\hat{H}_{\text{eff}} = \sum_k \mathbf{c}^\dagger(k) \mathbf{H}_{\text{eff}}(k) \mathbf{c}(k)$, where $\mathbf{c}(k) := (\hat{c}_A(k), \hat{c}_B(k))^T$ with $\hat{c}_{A(B)}(k) = 1/\sqrt{L} \sum_j e^{-ikj} \hat{c}_{A(B),j}$ and $\mathbf{H}_{\text{eff}}(k) = h_1(k)\sigma_x + h_2(k)\sigma_y$, where $h_1(k) = J_1 + (J_2 + J_3) \cos(k) - i\gamma_2/2 \sin(k)$, $h_2(k) = (J_2 - J_3) \sin(k) + i\gamma_2/2 \cos(k) - i\gamma_1/2$. Here, σ_i with $i \in \{x, y, z\}$ are the Pauli matrices. Since the effective Hamiltonian has a sublattice symmetry $\sigma_z \mathbf{H}_{\text{eff}}(k) \sigma_z^{-1} = -\mathbf{H}_{\text{eff}}(k)$, we can define the \mathbb{Z} topological number of $\mathbf{H}_{\text{eff}}(k)$, given by the winding number $\omega_{\text{PBC}} = \oint \frac{dk}{4\pi i} \text{Tr}[\sigma_z \mathbf{H}_{\text{eff}}^{-1}(k) \frac{d}{dk} \mathbf{H}_{\text{eff}}(k)]$ [2]. The winding number can be similarly defined for OBC, ω_{OBC} ,

by generalizing the momentum integral in the PBC winding number, ω_{PBC} , to those with complex values along the generalized Brillouin zone. (See e.g., Refs. [5, 14] for details.)

First, we focus on the case where $\gamma_2 = 0$, $J_3 = 0$. Here, in PBC, the topological transition point is given by $J_1 = J_2 \pm \gamma_1/2$ or $J_1 = -J_2 \pm \gamma_1/2$ [4]. For OBC, the spectrum can be easily obtained by means of a similarity transformation S , such that H_{eff} and $\tilde{H}_{\text{eff}} := S^{-1}H_{\text{eff}}S$ share the same spectrum. By taking $S = \text{diag}(1, r, r, r^2, r^2, \dots, r^{L-1}, r^{L-1}, r^L)$ with $r = \sqrt{|(J_1 - \gamma_1/2)/(J_1 + \gamma_1/2)|}$ [4, 5], \tilde{H}_{eff} becomes the Hermitian SSH model with hopping parameters $\tilde{J}_1 = \sqrt{(J_1 - \gamma_1/2)(J_1 + \gamma_1/2)}$ and $\tilde{J}_2 = J_2$ provided that $|J_1| > |\gamma_1/2|$. The phase boundary between topological and trivial phases can then be obtained as (assuming $J_1 > 0$ without loss of generality):

$$J_1 = \sqrt{J_2^2 + \left(\frac{\gamma_1}{2}\right)^2} \quad \text{or} \quad \sqrt{-J_2^2 + \left(\frac{\gamma_1}{2}\right)^2}, \quad (12)$$

as shown in Fig. 2(b). The discrepancy between OBC and PBC phase diagrams is due to the NHSE as shown in Fig. 2(b) [2, 4, 5].

We numerically demonstrate below that the topological transition point in OBC given by Eq. (12) can be detected through the ES dynamics of a PBC system after a quench. In our simulation, we set the pre-quench state to be the ground state in the trivial phase of Eq. (11), in the Hermitian limit $\gamma_1 = 0$.

Figure 2(c) and (d) show the quench dynamics of ES for a PBC system. Here, in panel (c), the post-quench parameters are in the topologically non-trivial phase for both OBC and PBC. In panel (d), on the other hand, the parameters are chosen such that the post-quench system is in a trivial (non-trivial) phase for a OBC (PBC) system.

For the trivial to topological quench in Fig. 2(c), we observe four ES eigenvalues crossing exactly at the entanglement zero mode energy, $\xi = 0.5$, as they decay. In contrast, in Fig. 2(d), we do not observe any crossings between eigenmodes, which exponentially decay towards the steady state. In the SM [35], we have numerically confirmed that the presence and absence of ES zero-crossings is determined by the phase boundary of the effective Hamiltonian H_{eff} for OBC, given by Eq. (12). This demonstrates a remarkable feature: the ES only cares about the topology of the OBC spectrum. We have also confirmed that the presence (absence) of ES zero-crossings is unaffected by the strength of uniform on-site balanced gain and loss (that does not affect the topology of \hat{H}_{eff} but do give rise to a finite lifetime to the response to a local perturbation [18–20]), consistent with our expectation that the ES zero-crossings have a topological origin [35].

Finally, we consider the more general case with $\gamma_2 \neq 0$, $J_3 \neq 0$ and demonstrate that the above features re-

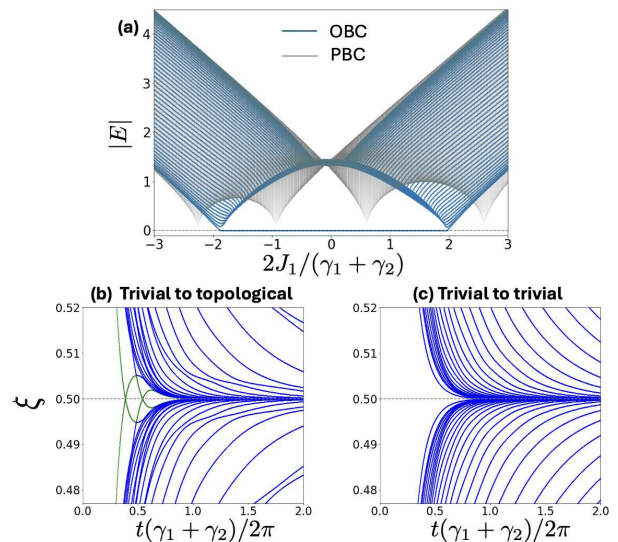


Figure 3. (a) The blue (grey) lines are the energy bands of the effective Hamiltonian H_{eff} in a finite open chain for $2J_2/(\gamma_1 + \gamma_2) = 1.4$, $2J_3/(\gamma_1 + \gamma_2) = 1/5$, $2\gamma_1/(\gamma_1 + \gamma_2) = 5/3$, $2\gamma_2/(\gamma_1 + \gamma_2) = 1/3$ in OBC (PBC). (b), (c) Quench dynamics of ES for PBC. The system is initially prepared in the trivial ground state of the SSH model $(J_2/J_1, J_3/J_1, \gamma_1/J_1, \gamma_2/J_1) = (0, 0, 0, 0)$, with system size $L = 50$, and a subsystem S of $M = 25$ sites. At $t = 0$ the relevant system ($S + \bar{S}$) is driven out of equilibrium by an abrupt change in parameters and allowing the system to couple to Markovian reservoirs at a rate γ_i , ($i = 1, 2$). (b) Trivial to topological quench for OBC and PBC spectrum $(2J_1/(\gamma_1 + \gamma_2), 2J_2/(\gamma_1 + \gamma_2), 2J_3/(\gamma_1 + \gamma_2)) = (-1, 1.4, 1/5)$. The green lines represent the four eigenvalues, $\xi_i(t)$, of the covariance matrix $C_{\text{SS}}(t)$ that is closest to $\xi = 0.5$ during the time evolution. The other eigenvalues are shown in blue. Two pairs of two ES eigenvalues, $\xi_i(t)$, cross $\xi = 0.5$ at different times as they decay. (c) Trivial to trivial (topological) quench for OBC (PBC) spectrum $(2J_1/(\gamma_1 + \gamma_2), 2J_2/(\gamma_1 + \gamma_2), 2J_3/(\gamma_1 + \gamma_2)) = (2.1, 1.4, 1/5)$. All the eigenvalues $\xi_i(t)$ shown in blue decay without zero-crossings.

main qualitatively intact even in cases where the effective Hamiltonian H_{eff} cannot be transformed to a Hermitian Hamiltonian. Figure 3(a) shows the single-particle spectrum of the effective Hamiltonian \hat{H}_{eff} for both OBC and PBC. Similarly to the previous case, we see that the topological transition point, marked by the closing of the energy gap, is different between OBC and PBC, again, due to the NHSE.

Figure 3(b) and (c) show the quench dynamics of ES for a PBC system, where, as before, we set the pre-quench state to be the ground state of the Hermitian SSH model in the trivial phase. In panel (b), the post-quench parameters lie in the topologically non-trivial phase for both OBC ($\omega_{\text{OBC}} = 1$) and PBC ($\omega_{\text{PBC}} = 1/2$), whereas for panel (c), quench parameters lie in the trivial phase for OBC ($\omega_{\text{OBC}} = 0$) and in the topological phase for PBC ($\omega_{\text{PBC}} = -1/2$). We observe that two pairs of

two ES eigenvalues, $\xi_l(t)$, crossing at $\xi = 0.5$ for the trivial to topological quench shown in Fig. 3(b), while Fig. 3(c) shows that no crossings occur for trivial to trivial quenches. This demonstrates that the presence or absence of zero-crossings in the ES dynamics is determined by the OBC phase diagram of the effective Hamiltonian H_{eff} .

We briefly note that, interestingly, the ES degeneracy at the crossing point occurring in the trivial to non-trivial quench case, seen in the absence of the next-nearest neighbor hopping $J_3 = 0$ (Fig. 2(c)) and in the Hermitian case [27] is lifted when $J_3 \neq 0$ in our open system case. We also observe that, for quenches on open chains, ES crossings remain degenerate. We do not have an explanation for these features, which remains our future work.

Conclusions.— In summary, our work has revealed that non-Hermitian topological phase transitions can be detected through the quench dynamics of the entanglement spectrum, specifically through the presence or absence of zero-crossings. Our results contribute to a deeper understanding of topological phases in open quantum systems.

Acknowledgments.— We thank Zongping Gong, Yuto Ashida, Kohei Kawabata, and Tianqi Chen for their helpful discussions. P. B.-P. acknowledges financial support from the Rotary Yoneyama Foundation and the Grant-in-Aid for Scientific Research No. 21H01006. He also thanks RIKEN for their warm hospitality during his stay there, where part of this work was initiated. RH was supported by the Grant-in-Aid for Research Activity Start-up from JSPS in Japan (Grant No. 23K19034). TM acknowledges support by JSPS KAKENHI Grant Numbers JP21H05185 and by JST, PRESTO Grant No. JPMJPR2259. HH was supported by the Kyoto University Foundation.

[1] Z. Gong, Y. Ashida, K. Kawabata, K. Takasan, S. Higashikawa, and M. Ueda, *Physical Review X* **8**, 031079 (2018).
 [2] K. Kawabata, K. Shiozaki, M. Ueda, and M. Sato, *Phys. Rev. X* **9**, 041015 (2019).
 [3] H. Shen, B. Zhen, and L. Fu, *Phys. Rev. Lett.* **120**, 146402 (2018).
 [4] S. Yao and Z. Wang, *Phys. Rev. Lett.* **121**, 086803 (2018).
 [5] K. Yokomizo and S. Murakami, *Phys. Rev. Lett.* **123**, 066404 (2019).
 [6] S. Yao, F. Song, and Z. Wang, *Phys. Rev. Lett.* **123**, 170401 (2019).
 [7] T. Haga, M. Nakagawa, R. Hamazaki, and M. Ueda, *Phys. Rev. Lett.* **127**, 070402 (2021).

[8] T. Mori, T. Shirai, *Phys. Rev. Lett.* **125**, 230604 (2020).
 [9] S. Hamanaka, K. Yamamoto, and T. Yoshida, *Phys. Rev. B* **108**, 155114, (2023).
 [10] N. Okuma, K. Kawabata, K. Shiozaki, and M. Sato, *Phys. Rev. Lett.* **124**, 086801 (2020).
 [11] K. Imura and Y. Takane, *Phys. Rev. B* **100**, 165430 (2019).
 [12] L. Xiao, et al., *Nature Physics* **16**, 761–766 (2020).
 [13] R. Shen, T. Chen, B. Yang, C.H. Lee, arXiv:2311.10143.
 [14] Z. Yang, K. Zhang, C. Fang, and J. Hu, *Phys. Rev. Lett.* **125**, 226402 (2020).
 [15] S. Longhi, *Phys. Rev. B* **102**, 201103 (2020).
 [16] N. Okuma and M. Sato, *Phys. Rev. Lett.* **126**, 176601 (2021).
 [17] L. Mao, T. Deng, P. Zhang, *Phys. Rev. B* **104**, 125435 (2021).
 [18] G. Lee, A. McDonald, and A. A. Clerk, *Phys. Rev. B* **108**, 064311 (2023).
 [19] A. McDonald, R. Hanai, and A. A. Clerk, *Phys. Rev. B* **105**, 064302 (2022).
 [20] S. E. Begg and R. Hanai, *Phys. Rev. Lett.* **132**, 120401 (2024).
 [21] F. Yang, Q. Jiang, and E. J. Bergholtz, *Phys. Rev. Research* **4**, 023160 (2022).
 [22] G. Lindblad, *Commun. Math. Phys.* **48**, 119–130 (1976).
 [23] V. Gorini, A. Kossakowski, and E. C. G. Sudarshan, *J. Math. Phys.* **17**, 821 (1976).
 [24] H. Li and F. D. M. Haldane, *Phys. Rev. Lett.* **101**, 010504 (2008).
 [25] L. Fidkowski, *Phys. Rev. Lett.* **104**, 130502 (2010).
 [26] F. Pollmann, A.M. Turner, E. Berg, and M. Oshikawa, *Phys. Rev. B* **81**, 064439 (2010).
 [27] Z. Gong and M. Ueda, *Phys. Rev. Lett.* **121**, 250601 (2018).
 [28] C. Wang, et al., *Phys. Rev. Lett.* **118**, 185701 (2017).
 [29] M. McGinley and N.R. Cooper, *Phys. Rev. Lett.* **121**, 090401 (2018).
 [30] S. Sayyad, J. Yu, A. G. Grushin, and L. M. Sieberer, *Phys. Rev. Research* **3**, 033022 (2021).
 [31] E. Starchl and L. M. Sieberer, *Phys. Rev. Lett.* **129**, 220602 (2022).
 [32] E. Starchl and L. M. Sieberer, *Phys. Rev. Research* **6**, 013016 (2024).
 [33] W. P. Su, J. R. Schrieffer, and A. J. Heeger, *Phys. Rev. Lett.* **42**, 1698 (1979).
 [34] S. Lieu, M. McGinley, and N. R. Cooper, *Phys. Rev. Lett.* **124**, 040401 (2020).
 [35] See Supplemental Material for details.
 [36] I. Peschel, *J. Phys. A* **36**, L205 (2003).
 [37] For example, consider a system which has loss only (i.e., $\hat{G}_{j,s=1,2} = 0$) with the initial state given by an all-occupied state. In this case, the system keeps losing particles from the system and would eventually converge to a vacuum state. This situation gives rise to the ES crossing for a trivial reason: the ES at the initial state $\xi_l(t=0) = 1$ converge to $\xi_l(t \rightarrow \infty) = 0$, which gives rise to ES crossing $\xi_l(t) = 0.5$ at finite time t , irrespective of the topology of \hat{H}_{eff} .

SUPPLEMENTAL MATERIAL

Conditional and Unconditional Dynamics for Quadratic Lindbladians

In this section, we show that the dynamics of the correlation function is given by Eq. (5). We also discuss the subtle difference between the non-Hermitian Hamiltonian \hat{H}_{cond} that governs the null-jump conditioned dynamics and the effective Hamiltonian \hat{H}_{eff} that governs the unconditioned dynamics of a correlation function. The GKSL equation (1) can be rewritten as,

$$\begin{aligned} \partial_t \hat{\rho}(t) &= -i[\hat{H}, \hat{\rho}(t)] - \frac{1}{2} \sum_{\alpha} \{\hat{L}_{\alpha}^{\dagger} \hat{L}_{\alpha}, \hat{\rho}(t)\} - \frac{1}{2} \sum_{\alpha} \{\hat{G}_{\alpha}^{\dagger} \hat{G}_{\alpha}, \hat{\rho}(t)\} + \sum_{\alpha} [\hat{L}_{\alpha} \hat{\rho} \hat{L}_{\alpha}^{\dagger} + \hat{G}_{\alpha} \hat{\rho} \hat{G}_{\alpha}^{\dagger}] \\ &= -i\hat{H}_{\text{cond}} \hat{\rho}(t) + i\hat{\rho}(t) \hat{H}_{\text{cond}}^{\dagger} + \sum_{\alpha} [\hat{L}_{\alpha} \hat{\rho} \hat{L}_{\alpha}^{\dagger} + \hat{G}_{\alpha} \hat{\rho} \hat{G}_{\alpha}^{\dagger}] - \sum_{\alpha, i} |g_i^{\alpha}|^2 \hat{\rho}(t), \end{aligned} \quad (\text{S1})$$

where

$$\hat{H}_{\text{cond}} := \hat{H} - \frac{i}{2} \sum_{\alpha} (\hat{L}_{\alpha}^{\dagger} \hat{L}_{\alpha} - \hat{G}_{\alpha} \hat{G}_{\alpha}^{\dagger}) = \hat{H} - \frac{i}{2} (\hat{L} - \hat{G}). \quad (\text{S2})$$

The final term is called the jump term, describing the jump process where the number of particles in the relevant system ($S + \bar{S}$) changes. In the case where one post-selects the quantum trajectories with no jump processes, the dynamics are governed by a non-Hermitian Hamiltonian \hat{H}_{cond} .

For the unconditional dynamics that we are interested in, the equation of motion of the (j, i) component of the covariance matrix $[\mathbf{C}]_{j,i}(t) = \text{Tr}_{S+\bar{S}}[\hat{c}_i^{\dagger} \hat{c}_j \hat{\rho}(t)] = \langle \hat{c}_i^{\dagger} \hat{c}_j \rangle$ is obtained by substituting the master equation for the relevant system ($S + \bar{S}$) Eq. (1) in $i\partial_t \langle \hat{c}_i^{\dagger} \hat{c}_j \rangle$ such that,

$$\begin{aligned} i\partial_t [\mathbf{C}]_{j,i}(t) &= i\text{Tr}_{S+\bar{S}}[\hat{c}_i^{\dagger} \hat{c}_j \partial_t \hat{\rho}(t)] \\ &= \text{Tr} \left[\hat{c}_i^{\dagger} \hat{c}_j \sum_{a,b} H_{a,b} [\hat{c}_a^{\dagger} \hat{c}_b, \hat{\rho}(t)] + iL_{a,b} \left(\hat{c}_b \hat{\rho}(t) \hat{c}_a^{\dagger} - \frac{1}{2} \{ \hat{c}_a^{\dagger} \hat{c}_b, \hat{\rho}(t) \} \right) + iG_{a,b} \left(\hat{c}_a^{\dagger} \hat{\rho}(t) \hat{c}_b - \frac{1}{2} \{ \hat{c}_b \hat{c}_a^{\dagger}, \hat{\rho}(t) \} \right) \right] \\ &= \sum_{a,b} H_{a,b} \langle [\hat{c}_i^{\dagger} \hat{c}_j, \hat{c}_a^{\dagger} \hat{c}_b] \rangle + \frac{i}{2} \sum_{a,b} \left(L_{a,b} \langle [\hat{c}_i^{\dagger} \hat{c}_j, \hat{c}_b] \rangle + [\hat{c}_a^{\dagger}, \hat{c}_i^{\dagger} \hat{c}_j] \langle \hat{c}_b \rangle + G_{a,b} \langle \hat{c}_b [\hat{c}_i^{\dagger} \hat{c}_j, \hat{c}_a^{\dagger}] + [\hat{c}_b, \hat{c}_i^{\dagger} \hat{c}_j] \hat{c}_a^{\dagger} \rangle \right). \end{aligned} \quad (\text{S3})$$

Using the algebra of fermionic operators $\{\hat{c}_i^{\dagger}, \hat{c}_j\} = \delta_{i,j}$, $\{\hat{c}_i, \hat{c}_j\} = 0$, we obtain

$$i\partial_t [\mathbf{C}]_{j,i}(t) = \sum_a \langle \hat{c}_i^{\dagger} \hat{c}_a \rangle \left[H_{j,a} - \frac{i}{2} (L_{j,a} + G_{j,a}) \right] - \sum_a \langle \hat{c}_a^{\dagger} \hat{c}_j \rangle \left[H_{a,i} + \frac{i}{2} (L_{a,i} + G_{a,i}) \right] + iG_{i,j}. \quad (\text{S4})$$

which is equivalent to Eq. (5), where the effective Hamiltonian is given by,

$$\hat{H}_{\text{eff}} := \hat{H} - \frac{i}{2} (\hat{L} + \hat{G}). \quad (\text{S5})$$

Therefore, the dynamics of the correlation function are governed by \hat{H}_{eff} . Note the sign difference in front of \hat{G} compared to the conditional Hamiltonian \hat{H}_{cond} in Eq. (S2).

ES and Covariance Matrix Spectrum

We wish to obtain the relation between the spectrum of the reduced density matrix of the subsystem of interest S and the spectrum of the covariance matrix. As pointed out in the text, for free fermionic systems the reduced density matrix of the subsystem of interest is given by $\hat{\rho}_S = \text{Tr}_{\bar{S}} \hat{\rho} = e^{-\hat{H}_S} / \text{Tr}[e^{-\hat{H}_S}]$. Here, \hat{H}_S is the entanglement Hamiltonian and its spectrum as the single particle ES. Since the total system Hamiltonian is Gaussian, the reduced density matrix of the subsystem of interest S should remain Gaussian. This allows us to generically express the entanglement Hamiltonian as

$$\hat{H}_S = \sum_{n,m} h_{n,m} \hat{c}_n^{\dagger} \hat{c}_m. \quad (\text{S6})$$

Using Eq. (S6), the covariance matrix elements of the subsystem S are given by

$$[\mathbf{C}_{\text{SS}}]_{m,n} = \text{Tr}_S[\hat{c}_n^\dagger \hat{c}_m \hat{\rho}_S] = \frac{1}{Z_S} \text{Tr}_S[\hat{c}_n^\dagger \hat{c}_m e^{-\hat{H}_S}] \quad (n, m \in S). \quad (\text{S7})$$

Let $\{|\phi_l\rangle = f_l^\dagger|0\rangle\}$ be a basis that diagonalizes the entanglement Hamiltonian, such that $\hat{H}_S = \sum_l \epsilon_l \hat{f}_l^\dagger \hat{f}_l$, where $\hat{c}_n = \sum_l \phi_l(n) \hat{f}_l$ and $\hat{c}_n|0\rangle = \hat{f}_l|0\rangle = 0$. Substituting on Eq. (S7), we obtain

$$[\mathbf{C}_{\text{SS}}]_{m,n} = \text{Tr} \left[\sum_{\mu,\nu} \phi_\mu^*(n) \phi_\nu(m) \hat{f}_\mu^\dagger \hat{f}_\nu \exp\left(-\sum_l \epsilon_l \hat{f}_l^\dagger \hat{f}_l\right) \right] / \text{Tr} \left[\exp\left(-\sum_l \epsilon_l \hat{f}_l^\dagger \hat{f}_l\right) \right], \quad (\text{S8})$$

$$= \sum_l \phi_l(n)^* \phi_l(m) \frac{1}{e^{\epsilon_l} + 1}. \quad (\text{S9})$$

Diagonalizing \mathbf{C}_{SS} and using Eq. (S9) we obtain Eq. (4).

ES crossing is determined by the topology of \hat{H}_{eff} in OBC and is robust against local dissipation

Here, we numerically confirm that the ES crossing is determined by the topology of \hat{H}_{eff} in OBC. Figures S1(b) and (d) show the ES dynamics after a dissipative quench in the case where the post-quench parameters are chosen to be very close to the phase boundary of the topological transition of the OBC spectrum shown in Fig. S1(a). Here, as in the situation considered in the main text, the pre-quench state is chosen to be in a topologically trivial state. As shown, the zero-crossing of the ES (does not) occur when the post-quench parameters are topological (trivial). This demonstrates that the ES crossing probes the non-Hermitian bulk-boundary correspondence in a periodic system. Furthermore, we confirm below that this property is robust against local dissipation. This is motivated by the property that was pointed out recently [S18–S20] that the presence of the LSE generically does *not* imply that correlation functions have sensitivity to boundary conditions, especially in the presence of a local dissipation [S18–S20]. Intuitively, this can be understood as follows: a wave packet prepared in the middle of the bulk would not know about the boundary condition unless it hits the boundary. However, as long as the wave packet has a finite lifetime, it generically decays before it propagates to the edge. A natural question to ask is whether ES zero-crossings are also sensitive to such perturbations, which we confirmed negative. Figures S1(c) and (e) show the effects of adding local gain and loss with rate Γ described by the jump operators $\hat{L}'_{A(B),j} := \sqrt{\Gamma/2} \hat{c}_{A(B),j}$ and $\hat{G}'_{A(B),j} := \sqrt{\Gamma/2} \hat{c}_{A(B),j}^\dagger$ to the ES dynamics. As these onsite gains and losses are local, the added terms merely shift the effective Hamiltonian \hat{H}_{eff} in the imaginary axis and therefore do not change its topological properties. Here, we have assumed that the added loss and gain are balanced, to ensure that the system converges to an infinite temperature state, for the same reason we describe in the main text (See also Ref. [S30, S37]). We see that even when we perturb the system with these series of local system-environment interactions, the property that the presence of ES zero-crossings reflects the topology of \hat{H}_{eff} of the post-quench parameter remain robust even near the phase boundary.

Effective Hamiltonian for the Lindbladian SSH model

Here we give explicit expressions for the non-Hermitian effective Hamiltonian Eq. (2) which determines the dynamics of the covariance matrix. As mentioned earlier, we focus on the case where the matrices \mathbf{L}, \mathbf{G} corresponding to \hat{L} and \hat{G} satisfy $\mathbf{L} = \mathbf{G}$. Hence, the steady state is given by the infinite temperature state $C(\infty) = (1/2)\mathbf{1}_{2N,2N}$, where $\mathbf{1}_{2N,2N}$ is the unit matrix of size $2N \times 2N$. From this, we can readily see that all ξ_l converge to 0.5 at $t \rightarrow \infty$. The formal solution of Eq. (5) is given by

$$C(t) = C(\infty) + e^{-iH_{\text{eff}}t} \left(C(0) - C(\infty) \right) e^{iH_{\text{eff}}^\dagger t}. \quad (\text{S10})$$

Due to the Gaussian nature of the initial state and its time evolution, the ES can be straightforwardly obtained by diagonalizing the covariance matrix restricted to the region S, C_{SS} . The effective (non-Hermitian) Hamiltonian reads

$$H_{\text{eff}} = \begin{pmatrix} -i(\gamma_1 + \gamma_2)/2 & J_1 + \gamma_1/2 & 0 & J_3 & 0 & 0 & \dots \\ J_1 - \gamma_1/2 & -i(\gamma_1 + \gamma_2)/2 & J_2 + \gamma_2/2 & 0 & 0 & 0 & \dots \\ 0 & J_2 - \gamma_2/2 & -i(\gamma_1 + \gamma_2)/2 & J_1 + \gamma_1/2 & 0 & J_3 & \ddots \\ J_3 & 0 & J_1 - \gamma_1/2 & -i(\gamma_1 + \gamma_2)/2 & J_2 + \gamma_2/2 & 0 & \ddots \\ \vdots & \vdots & \ddots & \ddots & \ddots & \ddots & \ddots \end{pmatrix}. \quad (\text{S11})$$

To obtain the ES of the subsystem S we numerically evaluate $C(t)$ and obtain ξ_l from the spectrum of $C_{SS}(t)$. The initial covariance matrix $C(0)$ is given by $[C]_{j,i}(0) = \langle GS | \hat{c}_i^\dagger \hat{c}_j | GS \rangle$, where $|GS\rangle$ is the ground state of the relevant system ($S + \bar{S}$) in the Hermitian limit. For translationally invariant systems, the many-body ground state wavefunction $|GS\rangle$ is a single Slater determinant of all single-particle eigenstates of \hat{H} with energies less than the Fermi energy $\epsilon_F = 0$, $|GS\rangle = \prod_{k;\epsilon(k)<0} \sum_{\alpha} (u_k^{\alpha} c_{\alpha}^{\dagger}(k)) |0\rangle$, where $|0\rangle$ is the vacuum state, $|\alpha, k\rangle = c_{\alpha}^{\dagger}(k) |0\rangle$, $u_k^{\alpha} = \langle \alpha, k | \psi(k) \rangle$ ($\alpha \in \{A, B\}$), and $\hat{H}|\psi(k)\rangle = \epsilon(k)|\psi(k)\rangle$.

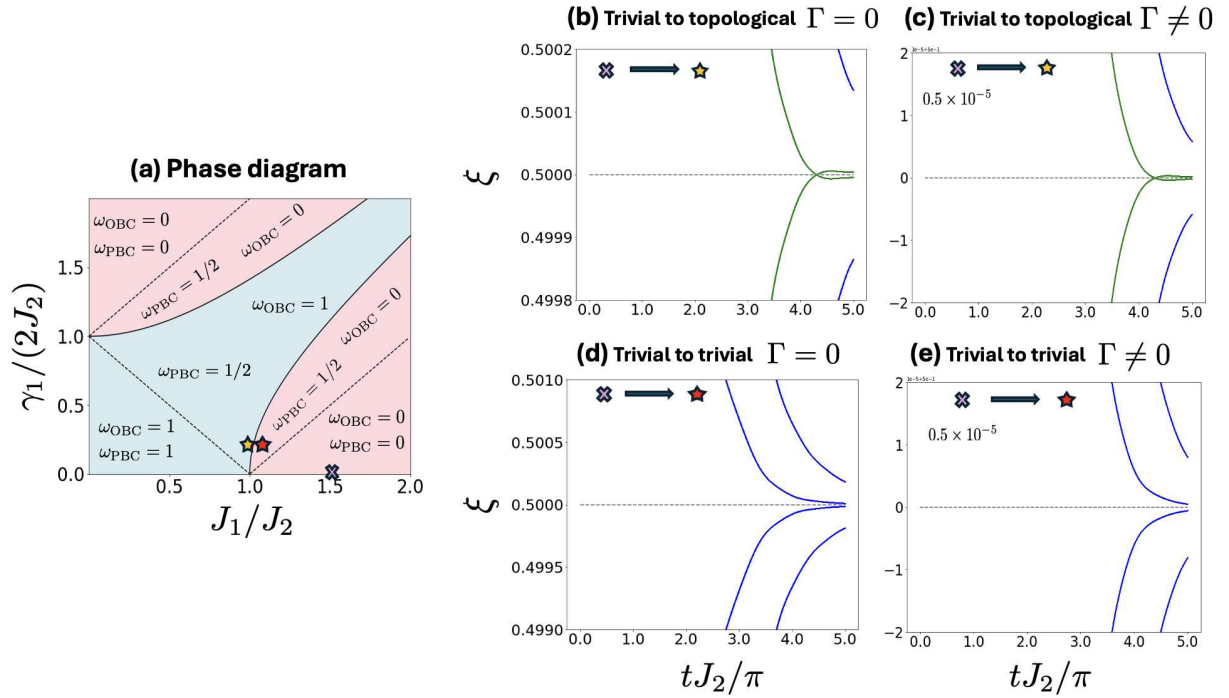


Figure S1. Quench dynamics of the ES for PBC. The system is initially prepared in the trivial ground state of the SSH model [S33] $(J_1/J_2, \gamma_1/(2J_2)) = (1.5, 0)$. Here we consider a system of 60 sites and a 10 sites subsystem S. (a) Phase diagram of the NH SSH model Eq. (11). Topological phase transitions are separated by the solid and dotted lines for OBC and PBC spectra, respectively. (b)-(e), Quench dynamics of ES for PBC. For trivial to topological quenches, the green lines represent the four eigenvalues, $\xi_i(t)$, of the covariance matrix $C_{SS}(t)$ that are closest to the zero energy entanglement value $\xi = 0.5$ during the time evolution. Eigenvalues away from $\xi = 0.5$ are shown in blue. (b) Trivial to topological phase quench without uniform dissipation $(J_1/J_2, \gamma_1/(2J_2), \Gamma/(2J_2)) = (1.009, 0.2, 0)$. (c) Trivial to topological phase quench with uniform dissipation $(J_1/J_2, \gamma_1/(2J_2), \Gamma/(2J_2)) = (1.009, 0.2, 0.1)$. (d) Trivial to trivial phase quench without uniform dissipation $(J_1/J_2, \gamma_1/J_2, \Gamma/J_2) = (1.029, 0.2, 0)$. (e) Trivial to trivial phase quench with uniform dissipation $(J_1/J_2, \gamma_1/J_2, \Gamma/J_2) = (1.029, 0.2, 0.1)$. All eigenmodes (blue lines) decay to $\xi = 0.5$ without crossing it.